Spin and band-gap engineering in doped graphene nanoribbons

Narjes Gorjizadeh,[1,*] Amir A. Farajian,[2] Keivan Esfarjani,[3] and Yoshiyuki Kawazoe[1]
[1]*Institute for Materials Research, Tohoku University, Sendai 980-8577, Japan*
[2]*Department of Mechanical and Materials Engineering, Wright State University, Dayton, Ohio 45435, USA*
[3]*Department of Physics, University of California–Santa Cruz, Santa Cruz, California 95064, USA*
(Received 11 August 2008; revised manuscript received 25 September 2008; published 27 October 2008)

We investigate electronic and magnetic properties of graphene nanoribbons whose edges are doped by *s*-, *p*-, and *d*-type atoms. The edges of the ribbon are chemically active and can accommodate appropriate dopants to obtain different electronic and magnetic properties, all with the same geometrical structure of the ribbon. Dopings by Mg and B turn the semiconducting armchair ribbon into a metal, while Fe and Mn change it into a ferromagnet with a large magnetic moment. Doping of zigzag ribbon and implications for transport characteristics are also discussed. Our results suggest that the present structures are suitable for nanoelectronic and spintronic applications.

DOI: 10.1103/PhysRevB.78.155427 PACS number(s): 73.50.−h, 73.22.−f, 73.61.Wp

I. INTRODUCTION

Graphene has recently attracted much attention in both theoretical[1–6] and experimental[7–9] fields. The development of experimental techniques for fabrication of single-sheet graphene has provided practical tools to investigate the properties of a real two-dimensional (2D) system.[7] Graphene's unique properties, such as half-integer quantum Hall effect,[9,10] finite conductivity at zero carrier concentration,[9] and half metallicity,[2] make it a promising candidate for applications in nanoelectronic and spintronic devices. Graphene nanoribbons, which are slices of graphene, are quasi-one-dimensional (1D) structures. They can have different edge geometries including zigzag and armchair. The electronic structure of the ribbon depends on the edge geometry.[11–13]

Nanoribbons intrinsically have dangling bonds at the edges. Their linear combinations form some of the eigenstates near the Fermi energy, and hence determine the ribbon properties. These dangling bonds also provide active sites for chemical bonding, making the ribbons suitable for doping. As the unique properties of the ribbons are associated with their edge states, engineering the edge will affect the electronic and magnetic properties of the ribbon.[5,14,15] In this work we investigate a route for controlling and designing electronic and magnetic devices based on graphene nanoribbons, with wide range of properties, using the same structure mold. We suggest that by doping of the edges of the same ribbon with various atoms, from *s*-type to *d*-type transition metals (TMs), we can obtain various electronic and magnetic properties. In fact, the same ribbon doped with different dopants can be insulator, semiconductor, metal, ferromagnet, and antiferromagnet.

Experimentally, the edge dangling bonds of the graphene sheets and ribbons can be saturated by hydrogen through specific hydrogenation procedures. Doping with transition metals has been theoretically investigated for graphite,[16] carbon nanotubes,[17,18] and infinite graphene sheet.[19] Oxidization of the edge of zigzag ribbons has also been theoretically studied.[5]

Here, using *ab initio* techniques, we investigate the electronic and magnetic properties of graphene ribbons doped with: (i) *s*-type elements, H and Mg; (ii) *p*-type elements, B, N, O, and S; and (iii) 3*d*-type TMs, Ti, Cr, Mn, Fe, and Co. We have chosen an armchair-edge ribbon with $N=8$ dimer lines across its width,[11] whose pristine form is semiconductor. We report the stability of the doped structures and band gaps of spin-up and spin-down carriers, as well as their density-of-states (DOS) ratio at the Fermi energy. Our results show that B and Mg can turn the armchair ribbon into a metal, while N, O, and S make it an insulator. Armchair ribbons are nonmagnetic, but if they are doped with *d*-type TMs, they can become ferromagnet or antiferromagnet, or half metal or half semiconductor, depending on the type of the TM atom and density of doping. Ribbons doped with Co and Cr have the most stable structures with large ratios of spin-up to spin-down carriers. This makes them suitable for spintronic applications. We also show that Fe has the largest magnetic stability. In addition to armchair nanoribbon with $N=8$, we consider a zigzag ribbon with $N=5$ zigzag chains across its width.[11] This zigzag ribbon is almost of the same width as the armchair ribbon with $N=8$ ($\sim$8.5 Å). Edge doping of the zigzag ribbon with typical *s*-, *p*-, and *d*-type elements is also briefly discussed.

II. METHOD

All the calculations presented in this work are performed using spin-polarized first-principles plane-wave approach, based on the density-functional method, ultrasoft pseudopotentials,[20–22] and generalized gradient approximation for the exchange-correlation energy.[23] Two unit cells of armchair graphene ribbon with $N=8$ are embedded in a supercell with periodic boundary conditions. There is 10 Å lateral spacing between the neighboring ribbons, in order to avoid their interaction. The Brillouin zone is sampled with $1\times1\times8$ k points for optimization of the structures (force threshold=0.001 eV/Å), and a $1\times1\times260$ mesh is used to determine the DOS. In all the calculations, the cut-off energy for the plane-wave expansion is 400 eV. In magnetic structures, both ferromagnetic (FM) and antiferromagnetic (AF)

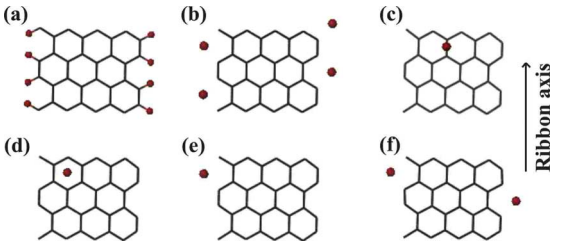

FIG. 1. (Color online) Schematic picture of different types of dopings for the armchair ribbon $N=8$. (a) is used for H doping; (b), (e), and (f) are coplanar edge dopings, while in (c) and (d) the dopant is on top of the ribbon.

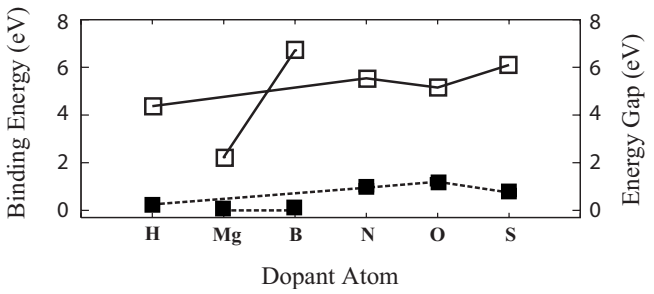

FIG. 2. Binding energy (solid line) and energy gap (dashed line) of armchair ribbon doped with different atoms. Doping geometries are those in Fig. 1(b) excluding that for hydrogen, which is in Fig. 1(a).

cases are optimized and their total energies are compared in order to obtain the most stable structure.

Different doping sites of the armchair ribbon are shown in Fig. 1. The dopant atoms are sketched as filled circles. These are the structures inside the supercells, and will be infinite in the direction of the ribbon axis. In the optimized structure of the pristine armchair ribbon, the C-C bonds at the edges are triple bonds with a length of 1.23 Å. In the doped structure in Fig. 1(a), the edge dangling bonds are saturated by hydrogen atoms. Therefore, the C-C bonds at the edges change into double bonds with a length of 1.37 Å. The C-H bond length in this case is 1.09 Å. Other dopants are situated either at the edge [(b), (e), and (f)] or on top [(c) and (d)]. In the case of N doping, with the schematic in Fig. 1(b), two unequal bonds are formed between each nitrogen and its two nearest carbon atoms. These bonds, with lengths of 1.29 and 1.48 Å, are located such that the short (long) bonds belonging to neighboring nitrogen atoms face each other. The short C-N bonds are so strong that the σ bonds between the corresponding C atoms of the edge are broken. The distance between these two C atoms is 2.57 Å. In order to investigate other doping possibilities and their properties, in Sec. IV, we also optimized the structures in Figs. 1(c)–1(f) for Fe.

III. DOPING WITH *s*- AND *p*-TYPE ATOMS

The pristine armchair nanoribbon $N=8$ is semiconductor with an energy gap of 0.45 eV. Doping this ribbon with H reduces the gap to 0.27 eV,[24] while dopants N, O, and S increase the gap to 0.92, 1.23, and 0.69 eV, respectively. These structures are insulators. However, Mg and B eliminate the gap and turn the ribbon into a metal. Binding energy per atom and energy gaps of these structures are depicted in Fig. 2. The binding energy per atom is calculated as

$$E_b = \frac{1}{n}(E_R + nE_D - E_{R+D}), \tag{1}$$

where E_R is the energy of an optimized pristine ribbon, n is the number of dopants in the supercell, E_D is the total energy of a free dopant, and E_{R+D} is the total energy for the optimized structure of the doped ribbon.

In a pristine nanoribbon the states near the Fermi energy are localized at the edges and are hence affected by edge doping. For doping with B, e.g., the B states, located above the Fermi energy, hybridize with the edge states and push them down the energy scale. Therefore the Fermi level crosses the conduction band and the ribbon becomes metallic. For N doping, however, the N state is below the Fermi energy and pushes the conduction band up. An asymmetric charge transfer in this case results in period doubling and opening of a gap.

According to Fig. 2, binding energies are more than 2 eV; thus these structures are thermally stable. The B-doped ribbon is more stable than Mg-doped one, which makes the former a better candidate for converting a semiconducting ribbon into a metallic one. None of these structures, which are doped with nonmagnetic atoms, shows magnetism.

IV. DOPING WITH 3*d*-TRANSITION-METAL ATOMS

The structure used for doping the ribbon with 3*d* TMs is the same as in Fig. 1(b). Ti, Cr, Mn, Fe, and Co atoms are positioned at the edges of the ribbon, and the structures are optimized. In all the optimized structures, the dopant atoms located at each edge are in ferromagnetic state. But the coupling of the doped atoms at the two opposite edges can be AF or FM. Therefore, we have done the optimizations in both AF and FM cases to compare the energies and find the most stable structure. All structures being metallic, no period doubling was observed after 3*d* doping. Figure 3(a) shows the binding energy per atom for the FM optimized case, and Fig. 3(b) depicts the difference in the binding energies between ferromagnet and antiferromagnet. According to this figure, the difference is negative for Ti and Cr, indicating that the ribbons doped with these two atoms are more stable in AF case. For Mn, Fe, and Co, the difference is positive, revealing that ribbons doped with these atoms have FM coupling. Fe has the strongest coupling, while Co and Cr are almost uncoupled.[25]

Our first-principles results show that for the armchair ribbon with $N=8$ and a width of ~8.5 Å, the exchange coupling between the two edges is positive for Mn and Fe, negative for Ti, and near zero for Cr and Co. Therefore the spin properties of the ribbon can be engineered by choosing a suitable combination of ribbon width and dopant type. These results may be understood in terms of a Ruderman-Kittel-Kasuya-Yosida (RKKY) model which predicts[6,26]

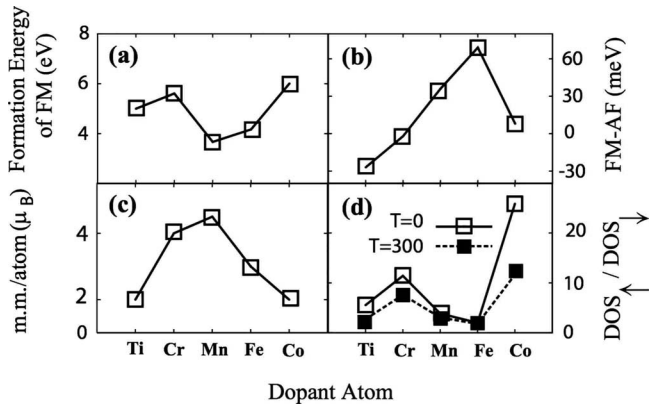

FIG. 3. (a) Binding energy per atom for FM states. (b) Differences in binding energy per atom between FM and AF states. (c) Magnetic moment per dopant atom for FM states. (d) DOS ratios of spin up and spin down at Fermi energy for zero and room temperatures. Doping geometries are those in Fig. 1(b).

$$J_{\mathrm{RKKY}} \propto -J^2 \int_q \chi^0(q)\cos(qR), \tag{2}$$

where J is the exchange interaction between the dopant atoms and the ribbon, χ^0 is the magnetic susceptibility of the pristine ribbon, and R is the distance between the spins. The RKKY interaction has an oscillatory behavior in terms of the width of the ribbon. The type of the dopant atom determines J^2. The charge transfer between the dopant atom and the ribbon and hence the Fermi momentum, which affect χ^0 and the period of oscillations, also depend on the type of dopants.

Transition metals interact with carbon atoms of the ribbon through their d-orbital electrons. As the spins of electrons of the half-filled $3d$ orbitals are parallel, the bonding of the TM will occur with the electrons of the carbons with the opposite spin. Therefore, the band structure of one of the spin channels is affected more than the other one. This effect makes the ribbon half metallic or half semiconducting due to TM doping. Figure 4 shows the band structure and the density of states of a ribbon doped with Fe. The two right plots are depicted for spin-up electrons, and the two left ones correspond to spin-down electrons. The band structure of spin up shows a wide gap at the Fermi energy, while the band structure of spin down has a number of flat bands due to $3d$ electrons of Fe. These d electrons are responsible for the metallicity of the doped ribbon.

The magnetic moment of all the structures in FM state is depicted in Fig. 3(c). Magnetic moments increase with increasing atomic number, up to Mn, and then decrease. This is because the number of unpaired electrons of the $3d$ orbitals increases with increasing atomic number until it reaches Mn, and then it decreases. These elements maintain more than 66% of their magnetic moments. The ratio of dopant (attached to ribbon) magnetic moment to that of the isolated atomic state is 100% for Ti, 67% for Cr, 90% for Mn, 75% for Fe, and 67% for Co. Therefore, the doped graphene ribbon provides large values of magnetization in a small area in one dimension, which is energetically and geometrically stable. For example, 1 nm of a ribbon doped with Mn (Fe)

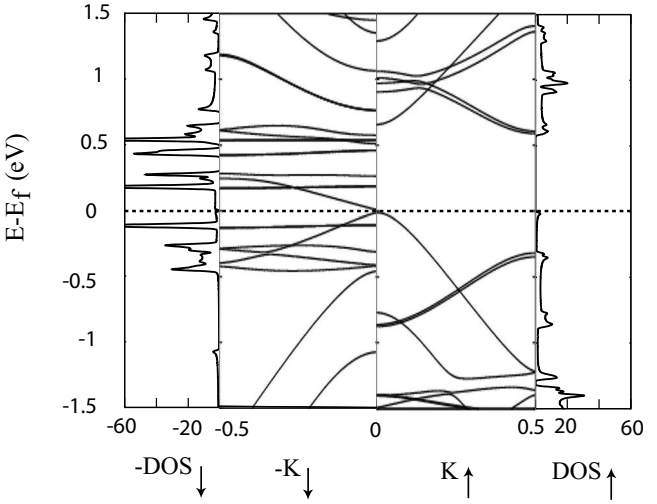

FIG. 4. Band structure and DOS of Fe-doped armchair ribbon [geometry in Fig. 1(b)]. The right two columns are for spin up and the left two columns with negative values are for spin down.

has a magnetic moment of $30\mu_B$ ($24\mu_B$). These structures could therefore be good candidates for spintronic and nanomagnetic applications.

Different behaviors of the FM spin-up and spin-down states are depicted in Fig. 3(d), where we show the ratio of $\mathrm{DOS}_\uparrow$ to $\mathrm{DOS}_\downarrow$ at Fermi energy for zero and room temperatures. The ratio at room temperature is calculated using the thermal DOS defined by

$$\mathrm{TDOS} = \int \mathrm{DOS}(E)\left[-\frac{\partial f(E)}{\partial E}\right]dE, \tag{3}$$

where f is the Fermi-Dirac distribution function. This ratio is higher for Cr- and Co-doped structures, which indicates that we can have spin-selective transport if we keep them in the FM state.

Up to now, the TM atoms were placed at the ribbon edge with highest possible density, i.e., as in Fig. 1(b). We also investigated other possible sites of Fe doping depicted in Figs. 1(c)–1(f). In the structures in Figs. 1(c) and 1(d) dopants are on top of the ribbon. The binding energies in Fig. 5 indicate that these two structures are not as stable as others,

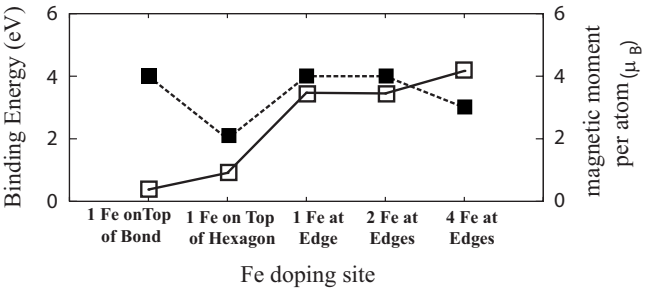

FIG. 5. Binding energy (solid line) and magnetic moment per dopant atom (dashed line) of Fe-doped armchair ribbon at different sites.

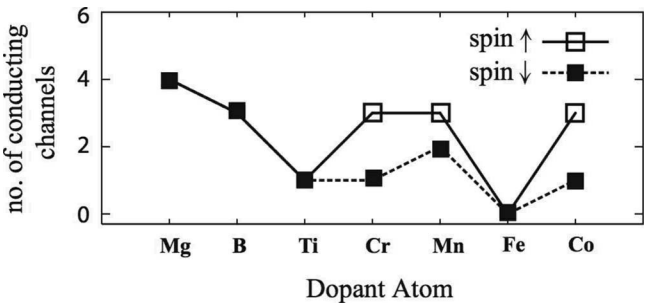

FIG. 6. Number of conducting channels for spin up and spin down for metallic doped armchair ribbon. Doping geometries are those in Fig. 1(b).

and the Fe atom in these positions may diffuse and attach to the ribbon edge. The binding energy of one Fe atom at the edge [Fig. 1(e)] is 3.47 eV. According to Fig. 5, if another Fe atom is attached to the other edge of the ribbon [Fig. 1(f)], the binding energy per dopant atom is the same. However, if there are two atoms attached to each edge, which is the structure in Fig. 1(b) with the highest possible concentration of Fe at the edge, the binding energy increases as a result of interaction between the neighboring Fe atoms. This is the most stable structure of the Fe-doped ribbon, and would be the most feasible structure experimentally. Therefore this doping geometry is the main one studied in this paper.

The magnetic moment per dopant atom for the five Fe-doped ribbons is shown in Fig. 5. The magnetic moment does not change from that of free atomic state of Fe for the cases where the Fe atom is placed on top of the C-C bonds and where it is attached to edge of the ribbon with low concentrations [Figs. 1(e) and 1(f)]. But if it is placed on top of the center of a hexagon, the magnetization reduces to $2\mu_B$. The reason is the change in hybridization of Fe from $4s^2 3d^6$ to $4s^0 3d^8$ for bonding with the six C atoms of the hexagon.[16,18] In the structure in Fig. 1(b), the magnetization reduces from $4\mu_B$ to $3\mu_B$, due to the interaction of Fe atoms. It is worth mentioning that the structure in Fig. 1(e) is half semiconductor, i.e., semiconductor with different energy gaps for spin up and spin down.[4] The energy gap is 0.31 eV for spin up and 0.01 for spin down. Interestingly, the structure in Fig. 1(f) is half metallic, with an energy gap of 0.61 eV for its semiconducting channel. These two structures are suitable for spintronic application, if they can be made by controlling the density of dopants.

V. CONDUCTANCE

As we showed, the ribbon can become metallic by doping with specific elements. In Fig. 6 we present the number of spin-up and spin-down conducting channels for the metallic doped ribbons. For nonmagnetic cases of Mg and B dopings, the numbers of conducting channels are equal for spin up and spin down. In the case of Fe doping, the number of conducting channels is zero, as this structure is semimetal, with zero DOS at the Fermi energy at zero temperature. At finite temperature, however, it becomes a conductor.

TABLE I. Binding energies (in eV) per dopant for Mg-, S-, Fe-, and Co-edge-doped armchair $N=8$ and zigzag $N=5$ nanoribbons. Doping geometries for the armchair ribbon are those in Fig. 1(b).

Dopant	Mg	S	Fe	Co
Armchair	2.23	6.10	4.17	6.02
Zigzag	2.12	5.69	4.34	6.10

VI. EFFECTS OF LARGER WIDTHS, ZIGZAG, AND MIXED EDGES

Based on previous *ab initio* results,[2] the band gap would be less than ~100 meV for ribbons wider than ~80 Å. Such wide ribbons basically approach the limit of infinite graphene sheet, whose "edge effects" are diminished. We therefore expect the modulation effects of edge doping to weaken for such wide ribbons. For the specific case of spin polarization, although the intraedge couplings are unaffected for wider ribbons, the interedge couplings diminish. The effect of dopant charge transfer on changing the Fermi level and hence the susceptibility of the ribbon diminishes while oscillating for wider ribbons, as does the relative strength of the exchange interaction J_{RKKY}. Although the magnetization of each edge remains intact, the total spin polarization upon edge doping is reduced due to a weakened interedge coupling and fluctuations. If the density of dopants is increased beyond the maximum edge-doping limit, however, the extra dopants would reside at "on-top" positions [Figs. 1(c) and 1(d)]. At such high dopant concentrations, therefore, it would be possible to observe modulation effects even for wider ribbons.

The binding energies of edge-doped zigzag nanoribbon $N=5$ are compared with those of edge-doped armchair nanoribbon $N=8$ in Table I. For edge doping of zigzag nanoribbon, our calculations show that the binding energies of *s* and *p* atoms Mg and S are less compared to the case of armchair nanoribbon. Doping the zigzag nanoribbon by the transition metals Fe and Co results in larger binding energies, compared to doping the armchair nanoribbon. The magnetic moments for the zigzag nanoribbon doped by Fe and Co are 3.1 and 1.8 μ_B/dopant, respectively, and the stable state is ferromagnet. These spin polarizations are similar to those of the armchair nanoribbon depicted in Fig. 3. We therefore expect that doping by transition metals would have similar (albeit slightly different) effects on a zigzag or mixed-edge nanoribbon.

The lower binding energies of Mg and S for the zigzag ribbon, as compared to the case of armchair ribbon, can be explained as follows. As Mg and S are group-II and -VI elements, respectively, they tend to make double bonds to complete their outer electronic shells. These double bonds can be provided by the edge dangling bonds of both armchair and zigzag ribbons. The edge dangling bonds of the zigzag ribbon are perpendicular to its axis. These bonds are needed to turn on their corresponding edge carbon atoms, which act as pivot points, to allow Mg or S binding. The corresponding elastic energy cost reduces the binding energy for zigzag ribbon. For the case of armchair ribbon, however, the edge dangling bonds are intrinsically tilted with respect to the rib-

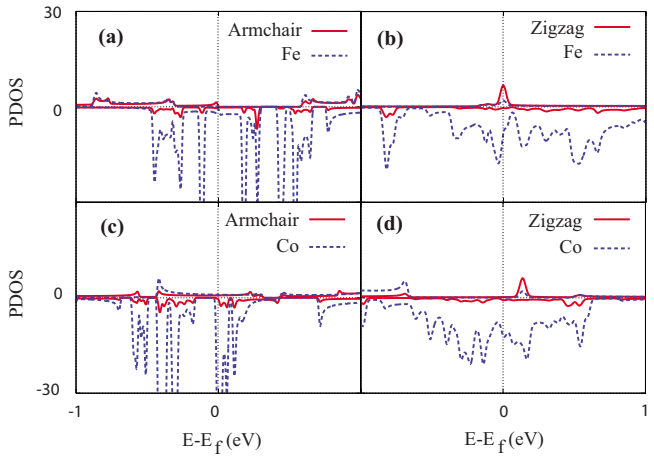

FIG. 7. (Color online) Spin-resolved PDOSs (arbitrary units) of a ribbon atom and the dopant, for armchair [Fig. 1(b)] and zigzag ribbons which are edge doped with Fe and Co.

bon's axis in such a way that they facilitate formation of bonds with Mg or S. The same explanation can apply to other group-II and -VI elements. Therefore, we expect the binding energies of these elements to be larger for armchair ribbon as compared to zigzag ribbon.

The case of transition metals is more elaborate owing to the contribution of their *d* states. Figure 7 shows the partial density of states (PDOS) for armchair and zigzag ribbons which are edge doped by Fe and Co. From Figs. 7(a) and 7(c), we observe that Co doping results in a larger degree of hybridization with armchair ribbon at and below Fermi energy, as compared to Fe doping. For armchair ribbon, therefore, the binding energy of Co is larger than that of Fe. This indeed agrees with the binding-energy results of armchair ribbon doping depicted in Fig. 3(a) and shown in Table I. The same is true for the zigzag ribbon doped with Fe and Co, as is evident from Figs. 7(b) and 7(d). The difference between the binding energies of Fe-doped zigzag and armchair ribbons is larger compared to the corresponding difference of Co-doped ribbons. This can be explained by the fact that Fe doping of the zigzag ribbon results in a distinctive PDOS peak at Fermi energy, which occurs at a higher energy for Co doping [Figs. 7(b) and 7(d)]. The difference in occupied states' hybridization between the zigzag and armchair cases is therefore larger for Fe doping as compared to Co doping.

The differences between dopings with Fe and Co arise from the electronic structure of these elements, combined with the edge geometries of the ribbons. A detailed analysis of the PDOSs of different atoms and states reveals that for the armchair ribbon doped with Co, the *s* and *d* states of Co bind strongly with the ribbon's states at the Fermi energy. For Fe, the *s*-state contribution occurs below Fermi energy and is almost the same for armchair and zigzag ribbons. The main difference between the armchair and zigzag ribbons doped with Fe is due to the above-mentioned distinctive PDOS peak corresponding to the *d* state of Fe and *p* state of the ribbon, which occurs at the Fermi energy of the doped zigzag ribbon.

VII. CONCLUSIONS

In conclusion, we have studied the properties of graphene ribbons doped with *s*, *p*, and *d* atoms. Based on our results we predict that B turns the semiconducting armchair ribbon into a metal, while N, O, and S enlarge the energy gap of the ribbon and make it insulator. Doping with 3*d* transition metals provides systems with FM or AF states at the edges. Armchair ribbons doped with Cr and Co have the most stable structures with large ratios of spin-up to spin-down density of states. These ribbons, however, are found to have small energy differences between their FM and AF states. The ribbon doped with Fe has the highest magnetic stability. Doping of the edge with low densities of Fe or Mn can result in half-semiconductor or half-metallic ribbon. Effects of width variation, zigzag edge, and edge uncertainty are also discussed. Therefore, graphene nanoribbons provide a wide range of possible electronic and magnetic properties based on the same ribbon structure but different dopant atoms.

ACKNOWLEDGMENTS

The authors would like to express their sincere thanks to the crew of the Center for Computational Materials Science, Institute for Materials Research, for their support of the Hitachi SR11000 (K2) supercomputer system. N.G. would also like to thank the Ministry of Education, Culture, Sports, Science and Technology of Japan and Global COE program of Tohoku University for financial support.

*narjes@imr.edu

[1] V. M. Pereira, F. Guinea, J. M. B. Lopes dos Santos, N. M. R. Peres, and A. H. Castro Neto, Phys. Rev. Lett. **96**, 036801 (2006).
[2] Y.-W. Son, M. L. Cohen, and S. G. Louie, Nature (London) **444**, 347 (2006); Phys. Rev. Lett. **97**, 216803 (2006).
[3] V. Barone, O. Hod, and G. E. Scuseria, Nano Lett. **6**, 2748 (2006).
[4] E. Rudberg, P. Sałek, and Y. Luo, Nano Lett. **7**, 2211 (2007).
[5] O. Hod, V. Barone, J. E. Peralta, and G. E. Scuseria, Nano Lett. **7**, 2295 (2007).
[6] L. Brey, H. A. Fertig, and S. Das Sarma, Phys. Rev. Lett. **99**, 116802 (2007).
[7] K. S. Novoselov, A. K. Geim, S. V. Jiang, Y. Zhang, S. V. Dubonos, I. V. Grigorieva, and A. A. Firsov, Science **306**, 666 (2004).
[8] Y. Zhang, Z. Jiang, J. P. Small, M. S. Purewal, Y. W. Tan, M. Fazlollahi, J. D. Chudow, J. A. Jaszczak, H. L. Stormer, and P. Kim, Phys. Rev. Lett. **96**, 136806 (2006).
[9] K. S. Novoselov, A. K. Geim, S. V. Morozov, D. Jiang, M. I. Katsnelson, I. V. Grigorieva, S. V. Dubonos, and A. A. Firsov, Nature (London) **438**, 197 (2005).

[10] Y. Zhang, Y. W. Tan, H. L. Stormer, and P. Kim, Nature (London) **438**, 201 (2005).
[11] M. Fujita, K. Wakabayashi, and K. Nakada, J. Phys. Soc. Jpn. **65**, 1920 (1996).
[12] R. Saito, M. Fujita, G. Dresselhaus, and M. S. Dresselhaus, Appl. Phys. Lett. **60**, 2204 (1992).
[13] D. J. Klein, Chem. Phys. Lett. **217**, 261 (1994).
[14] D. Gunlycke, J. Li, J. W. Mintmire, and C. T. White, Appl. Phys. Lett. **91**, 112108 (2007).
[15] E.-J. Kan, Z. Li, J. Yang, and J. G. Hou, J. Am. Chem. Soc. **130**, 4224 (2008).
[16] D. M. Duffy and J. A. Blackman, Phys. Rev. B **58**, 7443 (1998).
[17] M. Menon, A. N. Andriotis, and G. E. Froudakis, Chem. Phys. Lett. **320**, 425 (2000).
[18] Y. Yagi, T. M. Briere, M. H. F. Sluiter, V. Kumar, A. A. Farajian, and Y. Kawazoe, Phys. Rev. B **69**, 075414 (2004).
[19] K. T. Chan, J. B. Neaton, and M. L. Cohen, Phys. Rev. B **77**, 235430 (2008).
[20] G. Kresse and J. Hafner, Phys. Rev. B **47**, 558 (1993).
[21] G. Kresse and J. Hafner, Phys. Rev. B **49**, 14251 (1994).
[22] G. Kresse and J. Furthmüller, Phys. Rev. B **54**, 11169 (1996).
[23] J. P. Perdew, J. A. Chevary, S. H. Vosko, K. A. Jackson, M. R. Pederson, D. J. Singh, and C. Fiolhais, Phys. Rev. B **46**, 6671 (1992).
[24] This agrees with a previous observation for armchair ribbons of the same width (Ref. 3).
[25] Although 1D systems cannot have long-range order (LRO) in the thermodynamic limit, finite-length ribbons can display magnetic LRO at low enough temperatures.
[26] C. Kittel, Solid State Phys., Adv. Res. Appl. **22**, 1 (1968).